Estimating grassland dry mass in forage mixes using UAV imagery and PCR

Matheus Modesto Silva [1], Rebeca Campos Emiliano da Silva [2], Antonio Maria Garcia Tommaselli [2], Nilton Nobuhiro Imai [2]

[1] Graduate Program of Cartographic Sciences, Faculty of Sciences and Technology, São Paulo State University (UNESP) at Presidente Prudente, São Paulo, Brazil – (matheus.modesto, rebeca.campos)@unesp.br

[2] Department of Cartography, São Paulo State University (UNESP) at Presidente Prudente, São Paulo, Brazil – (a.tommaselli, nilton.imai)@unesp.br

Keywords: dry mass, forage mixes, grassland, PCR, UAV, Mavic 3M.

Abstract

Beef cattle farming is a significant activity in Brazil, and forage quality has a direct impact on animal performance. However, traditional methods for estimating dry mass, which involve cutting, drying and weighing plant material, are slow and labor-intensive. UAVs equipped with multispectral sensors, such as the DJI Mavic 3M, offer a faster and more scalable alternative for monitoring mixed-forage pastures. This study estimates the dry mass of forage mixtures using multispectral UAV data in two scenarios: (i) using only spectral information and (ii) combining spectral data with canopy height measured in the field. Model performance was evaluated using R^2, RMSE, and percentage error. The multispectral-only model explained 55% of dry mass variability (720.56 kg/ha; 23.67%), while adding canopy height improved performance to 80% and reduced the error to 589.41 kg/ha (19.36%). Results show that canopy height enhances the accuracy and operational potential of UAV-based methods for estimating dry mass in mixed-forage areas.

1. Introduction

1.1 Introduction

Beef cattle farming is one of the most significant economic activities in Brazil. This production system has benefited from Brazil’s favourable agricultural context, characterised by extensive territory, good soils, suitable climate conditions, and strong investment in agricultural research and development (Bungenstab and Almeida, 2014). As forage crops are the basis of cattle feed and their nutritional value varies according to species (Frota, 2015), it is essential to assess their quality to ensure proper animal growth. Forage quality assessment has been done manually by cutting, drying and weighing the collected material to determine dry mass, but these techniques are exhaustive, time-consuming and expensive over large areas.

The use of remote sensing and photogrammetry techniques, with unmanned aerial vehicles (UAVs) and lightweight multispectral sensors, such as the Mavic 3M UAV (DJI, 2024), shows potential for estimating forage evaluation parameters, including dry mass. Photogrammetric products can be generated from UAV images to extract three-dimensional and spectral metrics that serve as the basis for pasture parameter estimation models, as seen in da Silva et al. (2024) and Oliveira et al. (2020). The Structure from Motion (SfM) technique has proven to be an effective and low-cost approach for the three-dimensional image orientation and reconstruction of a scene from overlapping 2D images. The resulting multispectral mosaic and the Digital Surface Model can be used to estimate the height of agricultural crops (Viljanen et al., 2018).

Light Detection and Ranging (LiDAR) and Terrestrial Laser Scanning (TLS) technologies can also be used in agricultural applications, particularly in the stratified characterisation of the plant canopy. These sensors can penetrate vegetation and provide direct, detailed information on the three-dimensional structure of forage species with high precision. These characteristics make such active sensors valuable tools, given that canopy height shows a strong correlation with dry matter (Li et al., 2016). However, airborne and ground-based active systems generally result in higher costs when compared to multispectral sensors mounted on aerial platforms or UAV platforms.

This work aims to experimentally assess the estimation of the dry biomass of forage from different species and mixtures using multispectral data. Two scenarios are tested: (1) using only multispectral imagery and (2) combining spectral information with canopy height measurements obtained in the field. This approach seeks to provide a more efficient and scalable alternative to traditional manual methods for assessing forage quality.

2. Study area and data acquisition

The experiment was conducted on a farm intended for a crop-livestock integration system (ILP) and situated in the municipality of Caiuá, São Paulo, Brazil (21°51’29.41‘S, 51°57’27.84’W). The study area is 12 hectares in size and is divided into five plots (A1, A2, A4, A5, and A6). Each plot was planted with different forage species (Figure 1 and Table 1) and with ten sampling points. The collected samples were dried in an oven and weighed to determine dry mass, and canopy height was directly measured at each point. A homogenised sample was taken from each plot. At each plot, canopy height was measured twice, and the average was used as the representative value.

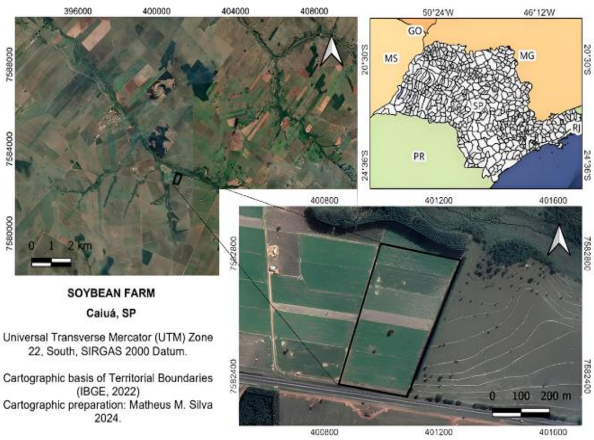

Figure 1. Location of the study area.

This contribution has been peer-reviewed.
https://doi.org/10.5194/isprs-archives-XLIX-B3-2026-1073-2026

Plot	Forage species	Mean	Standard deviation
A1	Brachiara ruziziensis	3157.43	1295.98
A2	Mix: BRS Piatã + B. ruziziensis	3113.68	1189.91
A4	Mix: BRS Marandu + BRS Xaraés	2737.15	1028.04
A5	BRS Marandu	2919.62	1021.61
A6	Mix: BRS Piatã + B. ruziziensis	3710.67	867.15

Table 1. Reference statistics (mean and standard deviation) of dry mass obtained for different forage species per plot.

RGB and multispectral sensors, measuring 1/2.8 and 4/3 inches respectively (Table 2), were used on the DJI Mavic 3M UAV (Figure 2a) to acquire the images, capturing data in the green (560 ± 16 nm), red (650 ± 16 nm), red edge (730 ± 16 nm), and near-infrared (860 ± 26 nm) bands. The flight campaign took place on April 30, 2024, at a flight height of 100 meters, with frontal and lateral overlap of 80% and 60%, respectively. In addition, to ensure precise positioning of the camera’s exposure stations, an RTK base (DJI D-RTK 2) was used and synchronised to the onboard receiver.

Sensor details	Multispectral	RGB
Field of view (FOV)	73.91° (61.2° × 48.10°)	84°
Focal length	4.34 mm	12.29
Aperture	f/2.0	f/2.8 a f/11
Type of focus	Fixed	1 m a ∞
Shutter speed	Electronic: 1/30 ~ 1/12.800 s	Electronic: 8-1/8000 s Mechanic: 8-1/2000 s
Pixel size	1.998 µm	3.358 µm
Image size	2592 × 1944 pixels	5280 × 3956 pixels
Image format	TIFF	JPEG/DNG

Table 2. Technical characteristics of the DJI Mavic 3M Sensor.

During image acquisition, radiometric calibration panels (Figure 2b), made of medium density fibreboard (MDF) and painted with acrylic material, were placed in the study area with the following colours: white, light grey, dark grey, and black. The radiance reflected by each of the four panel colours was measured using an ASD FieldSpec HandHeld spectroradiometer with a 1° lens and subsequently converted into reflectance values to assist in the radiometric calibration process.

Figure 2. (a) DJI Mavic 3M; (b) radiometric calibration panel.

For the georeferencing of the orthomosaics, control points were acquired using the RTK positioning method. In total, eight ground points were surveyed: six ground control points (GCPs) and two check points (CPs), with a horizontal accuracy of 9 mm and a vertical accuracy of 15 mm.

3. Methodology

3.1 Geometric processing

Metashape version 2.1.2 (Agisoft LLC, 2022) as used for phototriangulation, DSM and orthomosaic generation. The project parameters were defined with an initial accuracy of 20 cm and 2° for the exterior orientation parameters (EOP), comprising the camera position components (X, Y, Z) and the rotation angles (ω, φ, k). In addition, a precision 0.5 pixels was defined for the photo-coordinates and an accuracy of 2 cm for the GCPs. The reference system adopted was SIRGAS 2000, with UTM projection, Zone 22 South.

The geometric processing followed the workflow recommended by the manufacturer: (1) Initial image alignment, based on aerial triangulation (AT) and bundle block adjustment (BBA), to generate a sparse point cloud using the coordinates of the exposure stations determined by the RTK system; (2) Measurement of control points in the images and refinement of the initial alignment of the data, taking the ground control into account; (3) Manual and automatic removal of spurious and noisy points from the point cloud; (4) In situ calibration of the camera’s internal orientation parameters; (5) Creation of a dense point cloud from the sparse point cloud and the correspondence between points in the various images; (6) Generation of digital surface models (DSM) and digital terrain models (DTM); and (7) Generation of orthomosaics from the orthorectification of the original images of each band.

The orthomosaics were exported with a Ground Sample Distance (GSD) of 4.6 cm for each multispectral band (Figure 3c) and 2.7 cm for the RGB images (Figure 3b).

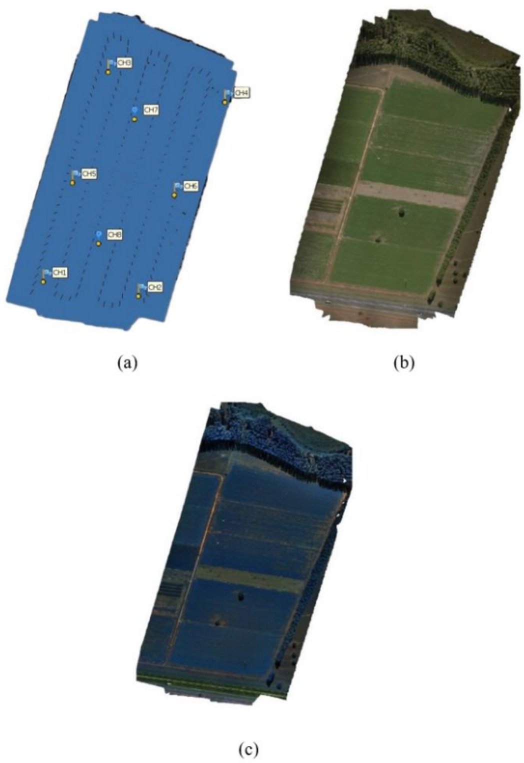

Figure 3. (a) Distribution of ground control points; (b) RGB ortho-mosaics, and (c) false-colour multispectral orthomosaic.

3.2 Radiometric processing

The radiometric calibration aims to convert the digital numbers (DNs) of the orthomosaics into physical reflectance values. To this end, the empirical line method (ELM) was adopted, based on a simple linear regression (Equation 1) between the mean DN values of the calibration plates and their corresponding reflectance values obtained in the field using a spectroradiometer. In Equation 1, (a) represents the slope (gain), while (b) represents the y-intercept (offset).

$$R = a \times DN + b \tag{1}$$

The determination of the empirical line requires the following tasks: (1) radiance measurements of the radiometric plates (white, light grey, dark grey and black), including a Spectralon type reference plate with a spectroradiometer; (2) conversion of these measurements into a reflectance factor, taking into account the radiance reflected by the target of interest (L_T) and by the reference plate (L_r), in the same spectral band, in addition to the application of a correction factor (k) (Equation 2) (Jensen, 2009); (3) simulation of optical sensor bands, considering their integrated spectral response, corresponding to a weighted average value based on bandwidth; (4) normalisation of the orthomosaics; (5) black level correction by subtracting the dark current value (3200 ND), as specified by the sensor manufacturer; and (6) extraction of average ND values using QGIS software version 3.34.35 (QGIS Development Team, 2023), from 5 × 5 pixel polygons (equivalent to 23 × 23 cm) defined over the calibration targets.

$$\rho_T = \frac{L_T}{L_r} \cdot k \tag{2}$$

Then, the calibration coefficients were calculated using Microsoft Excel, and these values were subsequently used to convert the orthomosaics to reflectance values using the *Raster Calculator* tool in QGIS. The absolute error (AE) analysis was used for the quality control of the empirical line adjustment.

3.3 Features extraction

The reflectance values for each band were extracted from the orthomosaics in the same position of the ground samples, using average values from a window with a radius of 28 pixels. From these values, 17 spectral indices (Table 3) were calculated using the R script (R Core Team, 2023) with the *RStoolbox* package (Müller et al., 2025). These spectral indices were selected based on their recognized use and validation in the literature for vegetation analysis.

3.4 Model and quality assessment

To assess the relationship between the explanatory variables and to test for multicollinearity, Pearson's correlation matrix was used. This approach allows us to understand the degree and linear relationship between pairs of variables, with coefficients ranging from -1 to 1 (Figueiredo Filho and Silva Junior, 2009).

Given the potential multicollinearity among the explanatory variables, Principal Component Regression (PCR) was used to estimate dry matter. This approach combines Principal Component Analysis (PCA) with multiple regression, transforming the highly correlated original variables into a new set of orthogonal components through linear combinations. A subset of these components, which explains most of the total variance in the data, is then used as an explanatory variable in the regression model, reducing dimensionality and multicollinearity (Hadi and Ling, 1998; Artigue and Smith, 2019).

It should be noted that the modelling stage was carried out using 19 samples from plots A1 and A5, since plots A2, A4 and A6 contained a mixture of cultivars. The dataset comprised 19 observations, with dry matter as the response variable and 21 explanatory variables (bands and indices). The samples were divided into 70% for training and 30% for testing.

Both the correlation analysis and the dry matter modelling stage were implemented in R using the *correplot* and *pls* packages, respectively. The estimation of dry mass was carried out in two scenarios: (1) without considering the canopy height variable, and (2) using canopy height measured in the field. The quality of the estimates in the three scenarios was assessed using the coefficient of determination (R^2), the root mean square error (RMSE) and the percentage error (RMSE%). In addition, the number of principal components used in the multiple regression for each scenario and the percentage of variance explained by each of them were analysed.

4. Results

4.1 Geometric processing

Table 5 shows the results of phototriangulation, indicating high quality of the bundle adjustment of multispectral block, with errors of less than one GSD in all components. Planimetric accuracy was higher than altimetric accuracy, as expected. Despite the consistent overall accuracy, the altimetric uncertainty may limit the precise estimation of canopy height. In addition, the generation of a Normalised Digital Surface Model was not reliable enough due to the variations in the bare soil surface. Due to these issues, grass heights directly measured in the field were used in the estimation. In future works, a lidar sensor will be integrated to generate accurate DSM.

Stacked multispectral bands	X	Y	Z
RMSE (cm)	1.9	2.8	3.2
GSD error	0.4	0.6	0.7

Table 5. RMSE, GSD, and relative error of the geometric processing.

4.2 Radiometric calibration

The results of applying the empirical line method (ELM) focused on the linear correction of the multispectral bands, identifying the most suitable radiometric targets. In addition, a validation point (vegetation), independent of the adjustment and determined in the field, was used for quality control. Thus, the linear calibrations for the four multispectral bands were firstly performed considering the four radiometric targets.

It was observed that, in the green band, the white target was already saturated and, because of its use in the empirical line calibration, the light gray target exhibited apparent saturation, with digital number (DN) values close to 1 (normalized to a 16-bit scale). Consequently, it was decided to exclude the white target from the modelling, retaining the light grey target, as its inclusion would increase the slope of the line and affect the estimation of the validation point. For the other bands (red, NIR, and red edge), all four radiometric targets were retained.

The results obtained were 3.4%, 1.2%, 1.4% and 4.3% for the green, red, red-edge and NIR bands, respectively. Similar results

Spectral indices	Equation	Autor
Corrected Transformed Vegetation Index (CTVI)	$\frac{NDVI + 0.5}{\sqrt{\lvert NDVI + 0.5 \rvert}}$	Perry and Lautenschlager (1984)
Difference Vegetation Index (DVI)	$s \cdot nir - red$	Richardson and Wiegand (1977)
Global Environmental Monitoring Index (GEMI)	$A = \frac{2(nir^2 - red^2) + 1.5 \cdot nir + 0.5 \cdot red}{nir + red + 0.5}$ $GEMI = A \cdot (1 - 0.25 \cdot A) - \frac{red - 0.125}{1 - red}$	Pinty and Verstraete (1992)
Green Normalized Difference Vegetation Index (GNDVI)	$\frac{nir - green}{nir + green}$	Gitelson and Merzlyak (1998)
Kernel Normalized Difference Vegetation Index (KNDVI)	$tanh\left(\frac{nir - red}{nir + red}\right)^2$	Camps-Valls et al., (2021)
Modified Soil-Adjusted Vegetation Index (MSAVI)	$nir + 0.5 - (0.5 \cdot \sqrt{(2 \cdot nir + 1)^2 - 8 \cdot (nir - 2 \cdot red)})$	Qi et al. (1994)
Modified Soil-Adjusted Vegetation Index 2 (MSAVI2)	$\frac{2 \cdot (nir + 1) - \sqrt{(2 \cdot nir + 1)^2 - 8 \cdot (nir - red)}}{2}$	Qi et al. (1994)
Normalized Difference Vegetation Index (NDVI)	$\frac{nir - red}{nir + red}$	Rouse et al. (1974)
Normalized Difference Water Index (NDWI)	$\frac{green - nir}{green + nir}$	McFeeters (1996)
Normalized Ratio Vegetation Index (NRVI)	$\frac{\frac{red}{nir} - 1}{\frac{red}{nir} + 1}$	Baret et al. (1991)
Ratio Vegetation Index (RVI)	$\frac{red}{nir}$	Jordan (1969)
Soil-Adjusted Vegetation Index (SAVI)	$\frac{(nir - red) \cdot (1 + L)}{nir + red + L}$	Huete (1988)
Thiam's Transformed Vegetation Index (TTVI)	$\sqrt{\left\lvert \frac{nir - red}{nir + red} + 0.5 \right\rvert}$	Thiam (1997)
Transformed Vegetation Index (TVI)	$\sqrt{\frac{nir - red}{nir + red} + 0.5}$	Deering (1975)
Weighted Difference Vegetation Index (WDVI)	$nir - s \cdot red$	Richardson and Wiegand (1977)
Normalized Difference Red Edge Index (NDRE)	$\frac{nir - rededge}{nir + rededge}$	Gitelson and Merzlyak (1998)
Modified Chlorophyll Absorption in Reflectance Index (MCARI)	$((rededge - red) - (rededge - green)) \cdot \left(\frac{rededge}{red}\right)$	Daughtry (2000)

Table 4. Spectral indices.

were reported by Sun et al. (2025), who observed errors in the range of approximately 1% to 4% for validation targets, indicating that the results obtained are consistent.

4.3 Spectral correlation and model

To analyse the correlation between the input variables, Pearson's correlation matrix was applied (Figure 4), which allows the degree of association between pairs of variables to be assessed. The matrix shows positive correlations, with values close to +1, represented by shades of blue, and negative correlations, with values close to −1, represented in red.

https://doi.org/10.5194/isprs-archives-XLIX-B3-2026-1073-2026 | © Author(s) 2026. CC BY 4.0 License.

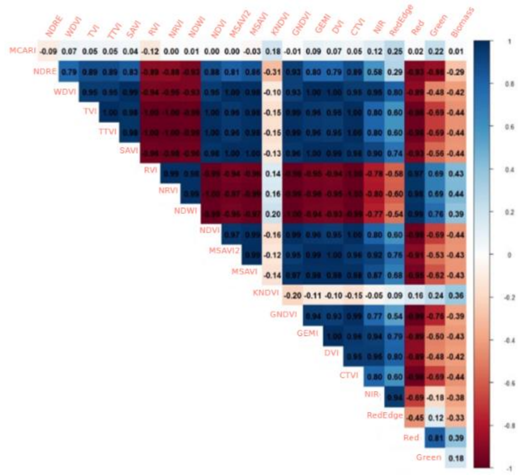

Figure 4. Pearson correlation matrix of spectral bands and vegetation indices.

The correlation matrix indicated that the spectral indices most positively correlated with grass biomass were the RVI (0.43) and the NRVI (0.44). The red band (0.39), the NDWI (0.39) and the KNDVI (0.36) also showed a significant positive correlation. However, the green band (0.18) and the red edge (0.12) showedweak correlations. Furthermore, several indices showed a negative correlation with biomass, such as NDVI (-0.44), SAVI (-0.44), TVI (-0.44), TTVI (-0.44), GEMI (-0.43), MSAVI (-0.43), MSAVI2 (-0.43), DVI (-0.42), WDVI (-0.42), GNDVI (-0.39) and NIR (-0.38).

When analysing the results for estimating grass biomass (Table 6), it was observed that, in scenario (i), the model explained 55% of the variability in dry matter, using two principal components, with a relative error of 23.67%. In scenario (ii), which includes grass height, however, the model performed better, explaining 80% of the variability with three principal components and a lower error (RMSE% of 19.36%), indicating higher precision in the estimates. This result reinforces the importance of grass height, as observed by da Silva et al. (2024).

Scenario	R^2	RMSE kg/ha	RMSE%	PC1%	PC2%	PC3%
i	0.55	720.56	23.67	78.55	91.52	-
ii	0.8	589.41	19.36	78.27	88.29	93.74

Table 6. Coefficient of determination (R^2), RMSE, and explained variance of principal components (PC%) of grass biomass models.

5. Conclusion

This study evaluated the use of multispectral imagery obtained by UAV to estimate the grass biomass of plots comprising different forage species. Four spectral bands, 17 vegetation indices and the average grass height in each plot were used as explanatory variables.

Although techniques based on three-dimensional models generated by photogrammetric techniques have potential for obtaining structural parameters, in this study we used direct measurements of grass height in the field due to the limited accuracy of the generated models by the mentioned indirect methods, which affected the quality of the height estimates.

A multiple regression model was used to estimate grass biomass based on spectral data and average grass height for each sample. However, as these variables are derived from spectral data, they tend to be highly correlated, since multiple bands and indices often capture similar information, leading to redundancy that may affect the interpretation of the results. In this context, Principal Component Regression (PCR) was adopted to reduce the dimensionality of the data and minimise multicollinearity, thereby improving the estimation of dry matter.

Results suggested that grass height is an essential parameter for estimating dry mass, explaining about 80% of the variability in dry mass values when incorporated into the model. In addition, the PCR regression technique proved effective in addressing the high correlation among the original variables.

For future work, we recommend developing a model to derive canopy height from photogrammetric products and applying methods to expand the sample set used in modelling. Depending on field conditions, using a Lidar sensor to provide reliable canopy height estimates is recommended. In addition, the use of multispectral sensors with more bands or hyperspectral sensors should be also assessed, combined with heights determined either by photogrammetric techniques or from Lidar sensor,

Acknowledgements

The authors would like to acknowledge the Conselho Nacional de Desenvolvimento Científico e Tecnológico - CNPq (Grant: 303670_2018-5) and the São Paulo Research Foundation, FAPESP (Grant: 2021/06029-7), CNPQ for granting the undergraduate research scholarship (process no. 136831/2024-9 and 308747/2021-6) and Coordenação de Aperfeiçoamento de Pessoal de Nível Superior – Brasil (CAPES) (88887.961785/2024-00).

References

Agisoft LLC, 2022. Agisoft Metashape software. agisoft.com (1 January 2024).

Artigue, H., Smith, G., 2019. The principal problem with principal components regression. Cogent Math. Stat., 6(1), 1622190. doi.org/10.1080/25742558.2019.1622190.

Baret, F., Guyot, G., Major, D.J., 1991. TSAVI: A vegetation index which minimizes soil brightness effects on LAI and APAR estimation. *Proc. IGARSS*, 1355–1358.

Bungenstab, D.J., Almeida, R.G., 2014. *Integrated crop-livestock-forestry systems: A Brazilian experience for sustainable farming*. Embrapa, Brasília, DF.

Camps-Valls, G., Campos-Taberner, M., Moreno-Martínez, Á., Walther, S., Duveiller, G., Cescatti, A., Mahecha, M.D., Muñoz-Marí, J., García-Haro, F.J., 2021. A unified vegetation index for quantifying the terrestrial biosphere. *Sci. Adv.*, 7(9), eabc7447. doi.org/10.1126/sciadv.abc7447.

da Silva, R.C.E., Tommaselli, A.M.G., Imai, N.N., Martins-Neto, R.P., da Silveira, D.D.S., Moro, E., 2024. Dry mass grassland estimation using UAV RGB images. *ISPRS Ann. Photogramm. Remote Sens. Spatial Inf. Sci.*, X-3, 69–75. doi.org/10.5194/isprs-annals-X-3-2024-69-2024.

Daughtry, C.S.T., Walthall, C.L., Kim, M.S., Brown de Colstoun, E., McMurtrey, J.E., 2000. Estimating corn leaf chlorophyll concentration from leaf and canopy reflectance.

Remote Sens. Environ., 74(2), 229–239. doi.org/10.1016/S0034-4257(00)00113-9.

Deering, D.W., 1975. Measuring “forage production” of grazing units from Landsat MSS data. *Proc. 10th Int. Symp. Remote Sens. Environ*., 1169–1178.

DJI, 2024. DJI Mavic 3M Multispectral – Specifications. ag.dji.com (16 November 2025).

Figueiredo Filho, D.B., Silva Junior, J.A., 2009. Desvendando os mistérios do coeficiente de correlação de Pearson (r). *Rev. Política Hoje*, 18(1), 115–146.

Frota, M.N.L., Carneiro, M.S.S., Carvalho, G.M.C., Araújo Neto, R.B., 2015. *Palma forrageira na alimentação animal*. Documentos 233, Embrapa Meio-Norte, Teresina, 47 p.

Gitelson, A.A., Merzlyak, M.N., 1998. Remote sensing of chlorophyll concentration in higher plant leaves. *Adv. Space Res.*, 22(5), 689–692. doi.org/10.1016/S0273-1177(97)01133-2.

Hadi, A.S., Ling, R.F., 1998. Some cautionary notes on the use of principal components regression. *Am. Stat.*, 52(1), 15–19. doi.org/10.1080/00031305.1998.10480530.

Huete, A.R., 1988. A soil-adjusted vegetation index (SAVI). *Remote Sens. Environ.*, 25(3), 295–309. doi.org/10.1016/0034-4257(88)90106-X.

Jensen, J.R., 2009. *Remote sensing of the environment: An Earth resource perspective*, 2nd ed. Pearson Education.

Jordan, C.F., 1969. Derivation of leaf area index from quality of light on the forest floor. *Ecology*, 50(4), 663–666. doi.org/10.2307/1936256.

Li, W., Niu, Z., Chen, H., Li, D., Wu, M., Zhao, W., 2016. Remote estimation of canopy height and aboveground biomass of maize using UAV stereo images. *Ecol. Indic.*, 67, 637–648. doi.org/10.1016/j.ecolind.2016.03.036.

McFeeters, S.K., 1996. The use of the Normalized Difference Water Index (NDWI) in the delineation of open water features. *Int. J. Remote Sens.*, 17(7), 1425–1432. doi.org/10.1080/01431169608948714.

Müller, K., Schwalb-Willmann, J., Wegmann, M., Leutner, B., 2025. RStoolbox: An R package for remote sensing data analysis. *Methods Ecol. Evol.*, 16, 486–495. doi.org/10.1111/2041-210X.14451.

Oliveira, R.A., Näsi, R., Niemeläinen, O., Nyholm, L., Alhonoja, K., Kaivosoja, J., Jauhiainen, L., Viljanen, N., Nezami, S., Markelin, L., Hakala, T., Honkavaara, E., 2020. Machine learning estimators for grass swards using drone-based imaging. *Remote Sens. Environ.*, 246, 111830. doi.org/10.1016/j.rse.2020.111830.

Perry, C.R., Lautenschlager, L.F., 1984. Functional equivalence of spectral vegetation indices. *Remote Sens. Environ.*, 14(1–3), 169–182. doi.org/10.1016/0034-4257(84)90013-0.

Pinty, B., Verstraete, M.M., 1992. GEMI: A non-linear index to monitor global vegetation. *Vegetatio*, 101, 15–20. doi.org/10.1007/BF00031911.

QGIS Development Team, 2023. QGIS Geographic Information System. Open Source Geospatial Foundation. qgis.org (1 January 2024).

Qi, J., Chehbouni, A., Huete, A.R., Kerr, Y.H., Sorooshian, S., 1994. A modified soil adjusted vegetation index. *Remote Sens. Environ.*, 48(2), 119–126. doi.org/10.1016/0034-4257(94)90134-1.

R Core Team, 2023. R: A language and environment for statistical computing. R Foundation for Statistical Computing, Vienna, Austria. r-project.org (19 April 2024).

Richardson, A.J., Wiegand, C.L., 1977. Distinguishing vegetation from soil background information. *Photogramm. Eng. Remote Sens.*, 43(12), 1541–1552.

Rouse, J.W., Haas, R.H., Schell, J.A., Deering, D.W., 1974. Monitoring vegetation systems in the Great Plains with ERTS. *NASA SP-351*, 309–317.

Sun, H., Guo, L., Zhang, Y., 2025. Accurate conversion of land surface reflectance for drone-based multispectral images. *Sensors*, 25(8), 2604. doi.org/10.3390/s25082604.

Thiam, A.K., 1997. GIS and remote sensing for land degradation assessment. *PhD Thesis*, Lund University, Sweden.

Viljanen, N., Honkavaara, E., Näsi, R., Hakala, T., Niemeläinen, O., Kaivosoja, J., 2018. Biomass estimation using drone data and machine learning. *Agriculture*, 8(5), 70. doi.org/10.3390/agriculture8050070.